ADVANCED MATERIALS

# Supporting Information

for *Adv. Mater.*, DOI: 10.1002/adma.201302066

# Phase Transitions, Phase Coexistence, and Piezoelectric Switching Behavior in Highly Strained $BiFeO_3$ Films

*C. Beekman, W. Siemons, T. Z. Ward, M. Chi, J. Howe, M. D. Biegalski, N. Balke, P. Maksymovych, A. K. Farrar, J. B. Romero, P. Gao, X. Q. Pan, D. A. Tenne, and H. M. Christen**

Submitted to ADVANCED MATERIALS

DOI: 10.1002/adma.201302066

**Supporting Information: Phase transitions, phase coexistence, and piezoelectric switching behavior in highly strained $BiFeO_3$ films**

By *C. Beekman, W. Siemons, T.Z. Ward, M. Chi, J. Howe, M.D. Biegalski, N. Balke, P. Maksymovych, A.K. Farrar, J. B. Romero, P. Gao, X.Q. Pan, D.A. Tenne, and H.M. Christen*[*]

Dr. C. Beekman, Dr. W. Siemons, Dr. T.Z. Ward, Dr. M. Chi, Dr. J. Howe, Dr. H.M. Christen
Materials Science and Technology Division, Oak Ridge National Laboratory, Oak Ridge, TN, 37831, USA
E-mail: christenhm@ornl.gov

Dr. M.D. Biegalski, Dr, N. Balke, Dr, P. Maksymovych,
Center for Nanophase Materials Sciences, Oak Ridge National Laboratory, Oak Ridge, TN, 37831, USA

Dr, A.K. Farrar, Dr, J. B. Romero, Prof. D.A. Tenne
Department of Physics, Boise State University, Boise, ID, 83725, USA

Dr. P. Gao, Prof. X. Q. Pan,
Department of Materials Science and Engineering, University of Michigan, Ann Arbor, MI, 48109, USA

Keywords: $BiFeO_3$, multiferroics, ferroelectric thin films, piezoelectric switching, phase transitions

**X-ray diffraction (XRD) measurements**

The temperature dependent XRD measurements were performed using a high temperature stage with a dome over the sample, allowing a flow of oxygen during heating. Here we note that the high temperature XRD measurements yielded the same results when heated in air or vacuum and that several temperature cycles (up to 600 °C) did not lead to a notable degradation of the sample.

*Temperature evolution of the monoclinic distortion:* In Fig. S1a and b we present the reciprocal space maps (RSM) for a 50 nm thick $BiFeO_3$ film grown on $LaAlO_3$ as function of temperature, with 25 °C < $T$ < 500 °C. The maps are taken through $103_{pc}$ and the $113_{pc}$ family of peaks. We extract the monoclinic angle $\beta$ and the $a/b$ ratio from the maps as follows: The angle $\beta$ is determined by the splitting of the triplet (doublet) in $q_z$, i.e. $\beta = \tan^{-1}(\Delta q_z/q_x)$. The $a/b$ ratio is determined by the ratio between the peak positions in $q_x$. In Fig. S1c we show the values for $\beta$ for different samples as function of temperature. The black squares correspond to the values extracted from Fig. S1 a and b for the 45 nm $BiFeO_3$ film grown on $LaAlO_3$ with a very low miscut. The blue triangles correspond to angles extracted from RSMs taken on a 100 nm thick film, the red stars correspond to angles extracted from RSMs taken on a 54 nm thick film grown onto a 10 nm thick $La_{0.7}Sr_{0.3}MnO_3$ bottom electrode and the green circles correspond to angles extracted from RSMs taken on a 40 nm thick film grown 4.5° miscut $LaAlO_3$. Important to note is that the values for the monoclinic angle and for the $a/b$ ratio measured on different films all coincide. The average of these values is shown in Fig. 2 a and b of the manuscript.

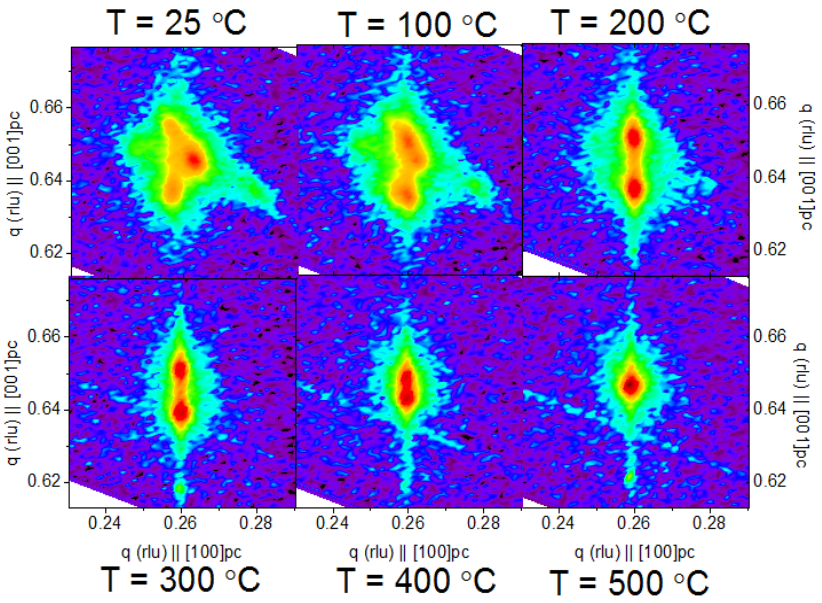


Fig. S1a: RSMs through the $103_{pc}$ family of peaks for a 45 nm thick $BiFeO_3$ film as a function of temperature from $T$ = 25 °C to $T$ = 500 °C.

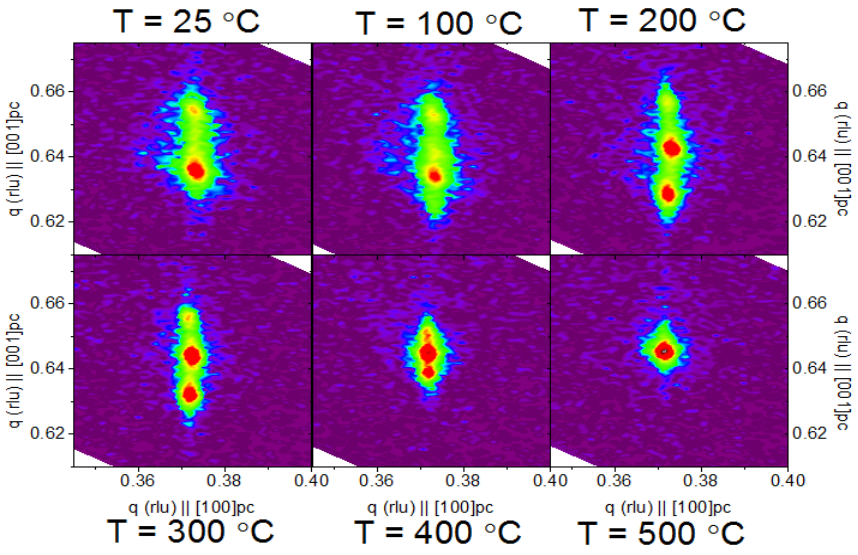


Fig. S1b: RSMs through the $113_{pc}$ family of peaks for a 45 nm thick $BiFeO_3$ film as a function of temperature from $T$ = 25 °C to $T$ = 500 °C.

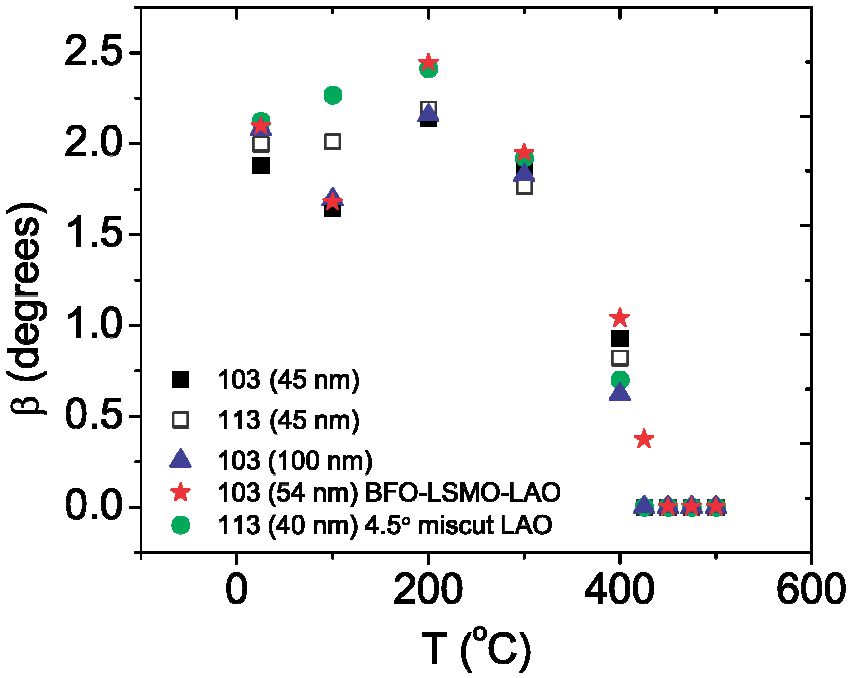


Fig. S1c: Monoclinic angle $\beta$ as a function of temperature determined for various samples. Black squares: 45 nm (103 peaks [closed] and 113 peaks [open]); blue triangles: 100 nm $BiFeO_3$ grown on very low miscut $LaAlO_3$ (103 peaks), red stars: 54 nm $BiFeO_3$ film grown on a $La_{0.7}Sr_{0.3}MnO_3$ bottom electrode (103 peaks); green circles: 40 nm $BiFeO_3$ film grown on 4.5° miscut $LaAlO_3$ (113 peaks).

*Temperature evolution of the S' polymorph:* maps through the $S'_{tilt}$ polymorph diffraction peaks in the (001) direction as function of temperature were also measured, with results shown in Fig. S2. Powder lines from the hot stage show up as horizontal "bands" of additional scatter intensity in these maps. The intensity of the $S'_{tilt}$ polymorph decreases with increasing temperature and fully disappears around 300 $^{o}$C.

More accurate intensities for this phase can be extracted from $\omega$ line-scans (see Fig. S3). The integrated intensities plotted in Fig. 2 c of the main text are determined from the $\omega$ line-scans taken through the (001) $S'_{tilt}$ (Fig. S3) and T' peaks (Fig. S4) as a function of temperature. To obtain the intensities we fitted the line-scans and extracted the diffraction peak areas (i.e. abundance) of the $S'_{tilt}$ and T'($M_C$, $M_A$) phases. The line-scans for the T'($M_C$, $M_A$) phase show additional peaks tilted away in $\omega$ with respect to the $LaAlO_3$ substrate (i.e. tilted T' phase). The positions and intensities of these peaks allow a determination of the amount of tilt and its abundance (Fig. 2c and d of the main text).

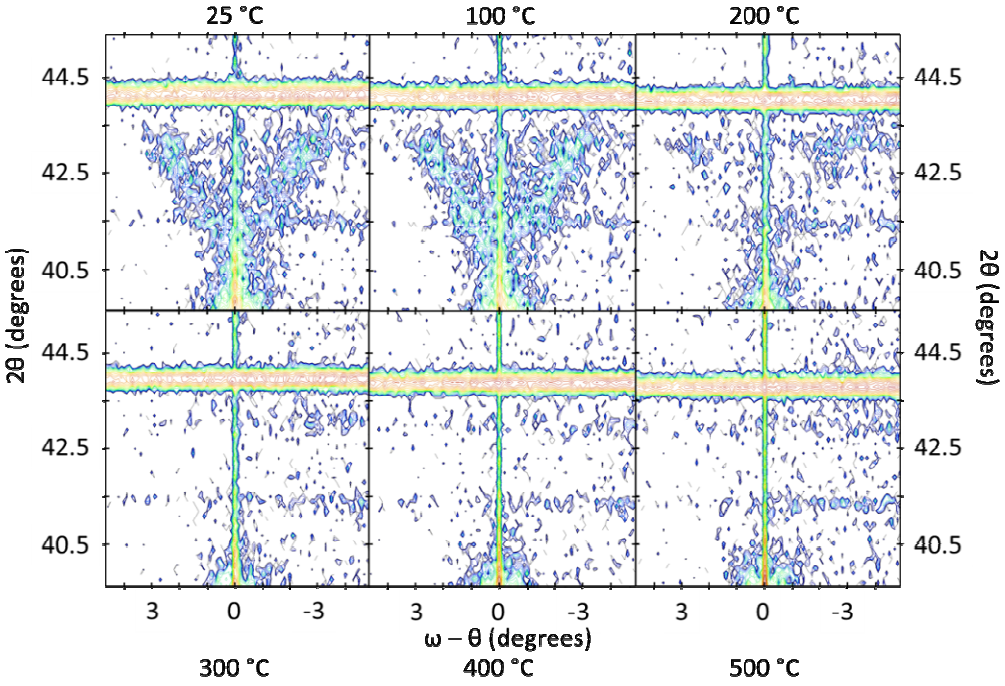


Fig. S2: X-ray ($2\theta$, $\omega$-$\theta$) maps through the (00l) diffraction peaks of the S' polymorph for a 45 nm thick $BiFeO_3$ film as a function of temperature from $T$ = 25 °C to $T$ = 500 °C.

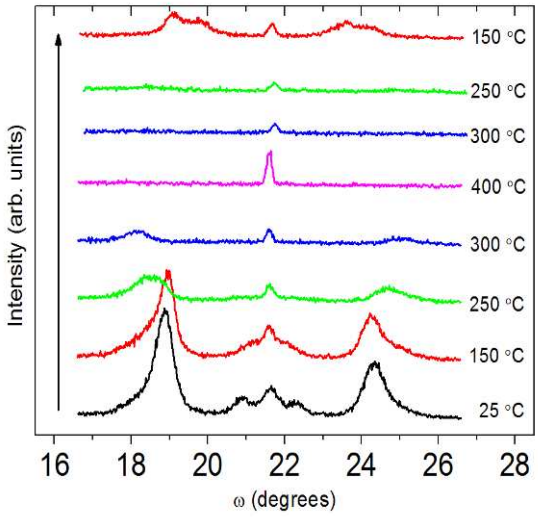


Fig. S3: $\omega$ line-scans taken through the (001) diffraction peaks ) of the S' polymorph as a function of temperature upon heating from $T$ = 25 °C to $T$ = 400 °C and returning to $T$ = 150 °C.

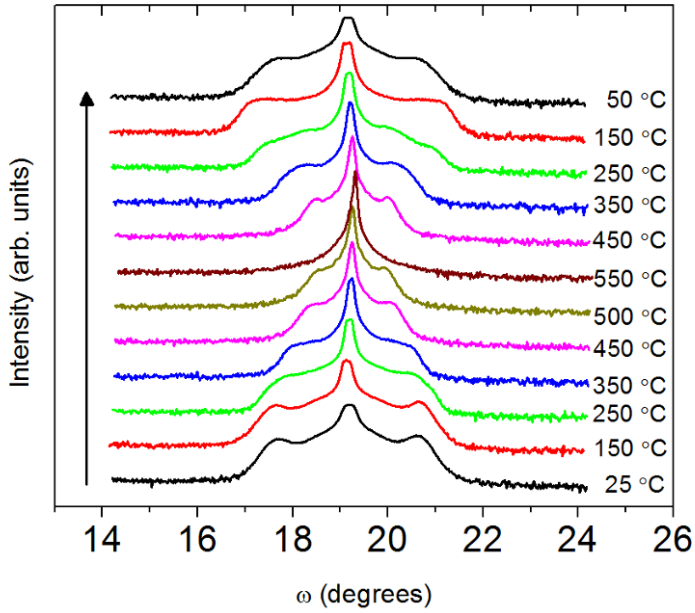


Fig. S4: $\omega$ line-scans taken through the (001) T'($M_C$,$M_A$) diffraction peaks as function of temperature.

**Piezoresponse force microscopy (PFM) and high temperature atomic force microscopy (AFM)**

PFM at room temperature confirm piezoelectric switching in the $BiFeO_3$ films. A bias of about 6-8 V had to be applied to switch the ferroelectric polarization of the film, which is originally poled with a "down" direction of the out-of-plane component. After poling several squares with opposite polarization direction we monitored the piezoresponse and the topography. The PFM phase image in Fig. S5a shows the poled regions. The images in Fig.S5b,c and d display the corresponding PFM amplitude, AFM topography and AFM deflection signal respectively, clearly showing the edges of the poled regions (dark) and the formation of the stripes consisting of $S'_{tilt}$ and $T'_{tilt}$ polymorphs at the ferroelectric domain boundary.

The local switching behavior is illustrated by the measurement of displacement, phase, and piezoresponse as shown in Fig. S5e. The typical butterfly loop clearly shows that the films can be switched. Switched domains remain stable for at least several days.

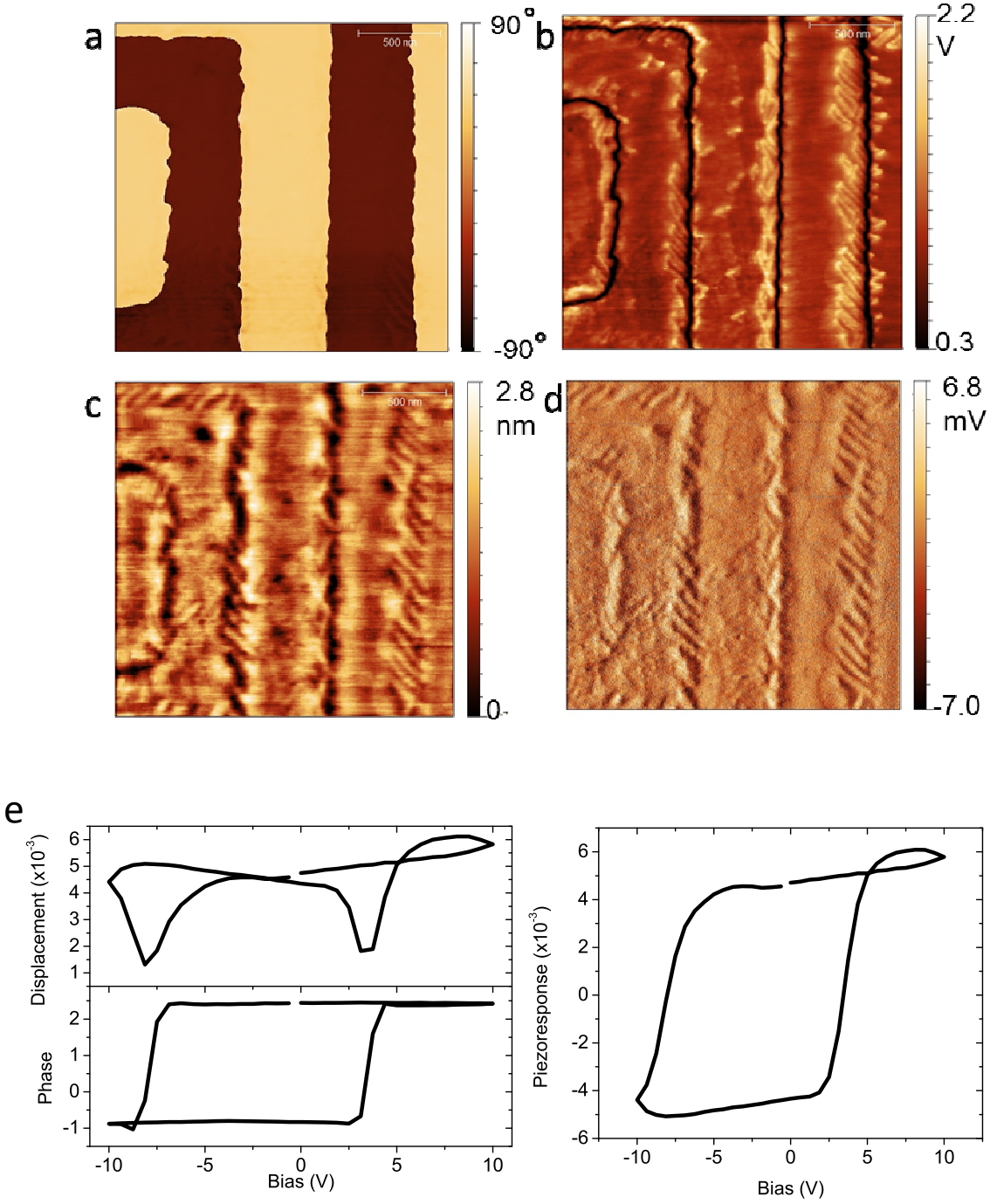


Fig. S5: a) PFM phase image after poling several regions of the film. b) Corresponding PFM deflection for the same region. c) AFM topography d) AFM deflection of the same region. The scan size for all images is 2 x 2 μm. e) Piezoelectric switching behavior, displacement, phase and piezoresponse at room temperature.

The high temperature AFM and PFM measurements were performed in ultra-high vacuum. Here we note that after multiple thermal cycles the conductivity of the film increased. Loss of oxygen from the film may be the reason for the observed increased conductivity at room temperature after 4 cycles and eventually the inability to switch the polarization. However, this did not prevent us from reproducibly establishing a clear temperature regime in which $BiFeO_3$ can be switched. We monitored the point-to-point switching probability across the sample as function of temperature by determining the number of successful loops at multiple temperatures. In Fig. S6 we show typical examples for loops that were fully successful (i.e. the ability to reversibly switch the region under the tip from the as-grown down state to the up-state and back to the down-state), loops that switched only in one bias direction (i.e. half loops) and loops for which no switching was observed.

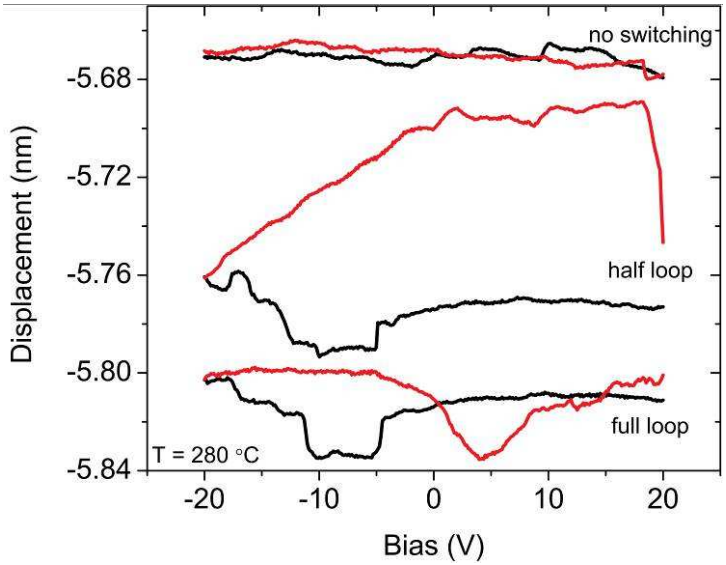


Fig. S6. Typical loops taken at $T$ = 280 °C for locations where switching was successful (full loop), for locations where switching only occurred in one bias direction (half loop) and for locations where switching was not observed (no switching).

We next investigate whether the inability to switch the $BiFeO_3$ film at elevated temperature could be due to lack of conductivity in the $La_{0.7}Sr_{0.3}MnO_3$ bottom electrode or due to increased conductivity in the film. To do so, we measured the lateral resistance of the $La_{0.7}Sr_{0.3}MnO_3$ bottom electrode as function of temperature on a part of the same sample that was used for the switching experiments. The 2-point resistance measurement shows a decrease of the resistivity with increasing temperature in the entire temperature range (25 – 500 °C, see Fig. S7a). Hence the $La_{0.7}Sr_{0.3}MnO_3$ electrode remains conducting throughout the temperature range in which the switching experiment was performed. Furthermore, we also measured the out-of-plane resistivity on the same $BiFeO_3$ film between a macroscopic top Pt electrode and the bottom $La_{0.7}Sr_{0.3}MnO_3$ electrode. The measured resistivity gradually decreases with increasing temperature consistent with the expected insulating behavior (see Fig. S7b). Also, no significant hysteresis was measured upon thermal cycling. The lack of sudden changes in the resistivity behavior clearly indicates that the absence of switching at elevated temperatures is not due to high conductivity of the $BiFeO_3$.

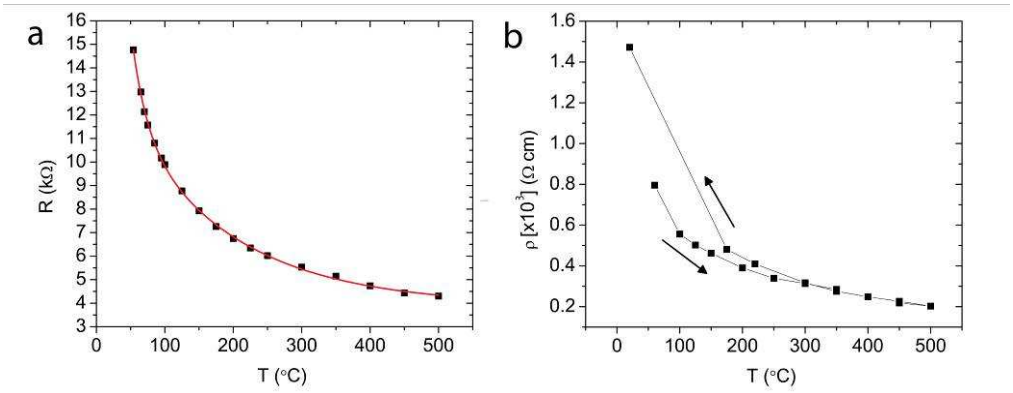


Fig. S7. a) Resistance versus temperature for a 10 nm $La_{0.7}Sr_{0.3}MnO_3$ bottom electrode. The red line is a fit. b) Resistivity vs. temperature across a 44 nm $BiFeO_3$ film between a top Pt electrode and the $La_{0.7}Sr_{0.3}MnO_3$ bottom electrode upon warming and cooling. Both measurements were performed in a pressure of $2x10^{-6}$ Torr.

**Ultraviolet Raman spectroscopy**

Raman spectra of $BiFeO_3$ films with the thicknesses of 100 nm and 40 nm have been measured in backscattering geometry normal to the film surface using a Jobin Yvon T64000 triple spectrometer equipped with a liquid nitrogen cooled multichannel charge coupled device detector. An ultraviolet excitation (325 nm line of He-Cd laser) was used for excitation in order to reduce the substrate contribution.[1] Maximum laser power density was ≈ 0.5 W/mm$^2$ at the sample surface, low enough to avoid any noticeable local heating of the sample.[1] Spectra were recorded in the temperature range 10–950 K using a variable temperature closed cycle helium cryostat and a high-temperature stage.

Bulk unstrained $BiFeO_3$ is rhombohedral in its ferroelectric phase below the $T_c \approx 1100$ K. It has a 10-atom unit cell, which belongs to the *R*3c space group. Vibrational spectra of rhombohedral $BiFeO_3$ have been characterized experimentally by Raman[2-7] and infrared[8-9] spectroscopy, as well as first principles lattice dynamical calculations.[10] The *R3c* primitive cell contains two $BiFeO_3$ formula units, resulting in 27 zone-center optical phonon modes: $4A_1+5A_2+9E$ modes (the latter are double degenerate). Of these modes, 13 are Raman-active: 4 $A_1$ and 9 *E* modes. Tetragonal phase of $BiFeO_3$ has the space group *P4mm* with 5 atoms per unit cell. Lattice dynamical properties of tetragonal $BiFeO_3$ have also been calculated from first principles.[11] The zone center optical phonons are $3A_1 + B_1 + 4E$ (the *E* modes are doubly degenerate), all of them can be Raman active.[6,12-13]

$BiFeO_3$ films commensurately grown on $LaAlO_3$ substrates are subject to ~4.4% compressive strain. According to the first-principles calculations,[14] at small strain values, the structure closely resembles the rhombohedral *R*3*c* bulk phase, although the substrate constraint causes a monoclinic distortion. Even though the symmetry is lowered from *R*3*c* to *Cc*, the distortion is small, and the structure can still to a good approximation be described as rhombohedral-like monoclinic. At strain values higher than 4%, the density-functional calculations predict the structure to become tetragonal-like with larger *c/a* ratio. This structure also has *Cc* symmetry, according to the first principles calculations,[14] but can be approximated by the tetragonal *P4mm* symmetry. The unit cell of *Cc* structure is base-

centered and contains four formula units, and the Raman-active phonon modes are 13*A*' + 14*A*".[6,12,15] Raman selection rules for the *R3c*, *P4mm*, and *Cc* structures are summarized in Refs.[12,15] For backscattering from the (001) surface, the *E* modes of the *P4mm* structure are forbidden, and only the $A_1$ modes are expected in Raman spectra. Therefore, one can expect the observation of only four (are $3A_1 + B_1$) modes in Raman spectra of the purely tetragonal *P4mm* phase, while many more lines (13*A*' + 14*A*") can be seen in the monoclinic (*Cc*) structure.

Temperature evolution of Raman spectra of the 100-nm thick $BiFeO_3$ film is shown in Fig. S8. The film thickness is large enough to absorb the UV light used for excitation almost completely, and the signal from $LaAlO_3$ substrate is mostly blocked, only one peak (at ~ 130 $cm^{-1}$ at room temperature) can be seen in the spectra. At low temperatures, we have observed at least 17 $BiFeO_3$ phonon peaks at ~70, 88, 110, 154, 188, 237, 255, 282, 317, 375, 415, 455, 495, 525, 560, 605, and 703 $cm^{-1}$ (Even though some peaks are weak, they are nevertheless reproducibly detectable). Most of the peaks are much stronger in parallel polarization configuration. Such large number of phonon modes indicates that the structure is monoclinically distorted (*Cc*), although 13 most intensive peaks are consistent with both the *A*' modes of the Cc structure, which are active in parallel polarization geometry.[12] Therefore, we assume the low-temperature phase of the films to be monoclinic.

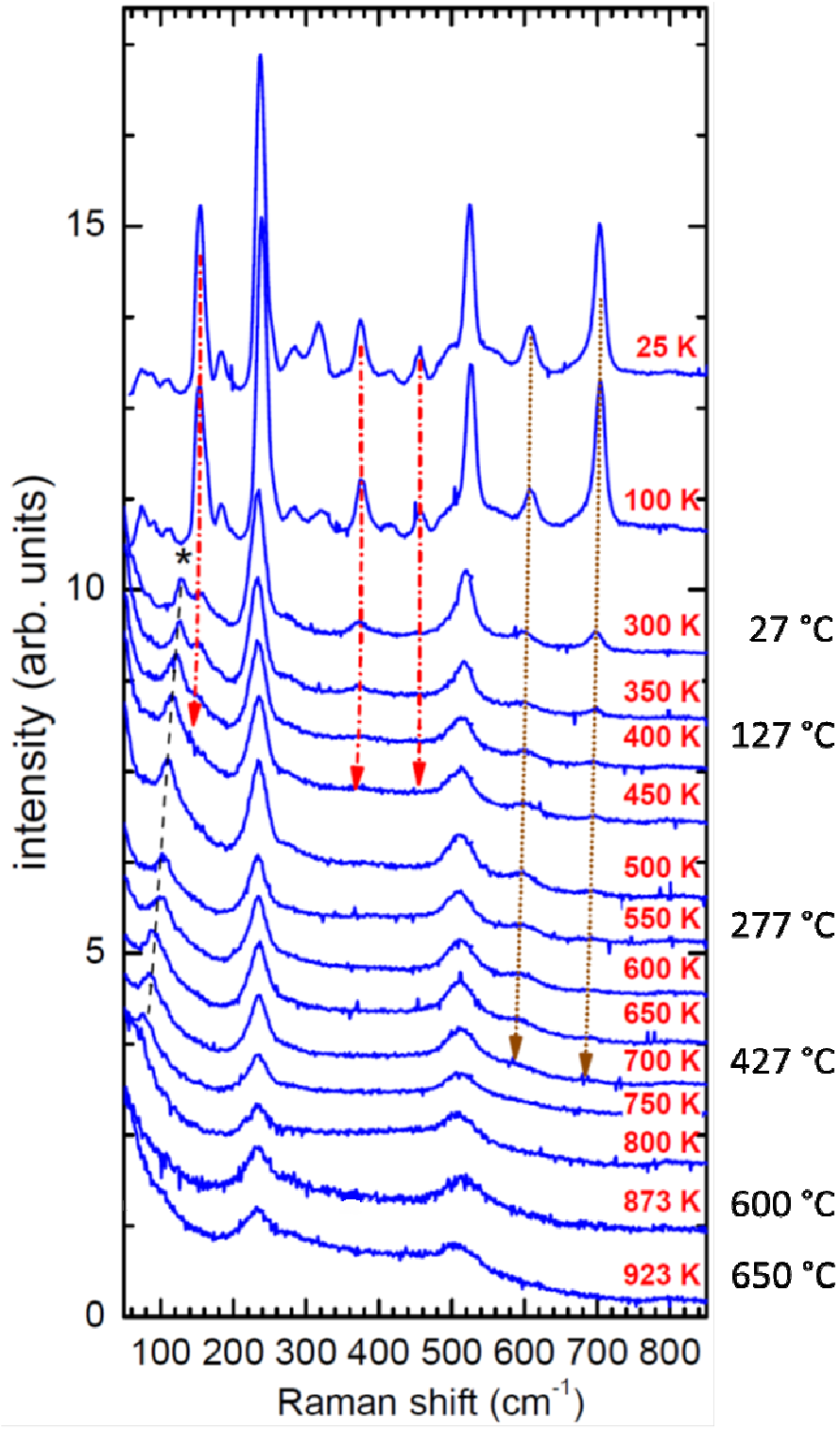


Fig. S8 Raman spectra of a 100-nm-thick $BiFeO_3$ film on $LaAlO_3$ as a function of temperature. Red dashed-dotted lines are guides to an eye indicating few phonon lines disappearing upon the T'($M_C$)-T'($M_A$) transition; brown dotted lines show phonon peaks indicative of the transition to purely tetragonal phase above 700 K. Black star and dashed line mark a line from $LaAlO_3$ substrate.

As can be seen from Fig. S8, with increasing temperature, the intensity of several phonon peaks of the $BiFeO_3$ films decreases, and the peaks disappear from the spectra above ~400 K, while other peaks disappear at higher temperature, ~700K. High-temperature spectra

(above 700 K) contain two features at about 235 and 515 $cm^{-1}$. This behavior indicates two structural phase transitions, near 400 K and 700K. The data for the 400K-transition is consistent with the monoclinic-to-monoclinic transition described in the main text. The higher temperature phase (above 700K) is tetragonal, since the phonon peaks active in *P4mm* structure remain in the high-temperature Raman spectra, while the other peaks disappear. This high-temperature phase is still polar (non-centrosymmetric), because a centrosymmetric phase would not have Raman active peaks at all.

The temperature of these phase transitions has been determined by plotting the normalized Raman intensity as a function of temperature for the peaks indicated by arrows in Fig. S8. The intensities were normalized by the Bose factor $n+1=(1-e^{-\hbar\omega/kT})^{-1}$ (here $\hbar$, $k$, $\omega$, and $T$ are the Planck's and Boltzmann's constants, the phonon frequency, and temperature, respectively), and divided by the intensity of the corresponding mode at 10 K.

***References***


[1] D. A. Tenne, A. Bruchhausen, N. D. Lanzillotti-Kimura, A. Fainstein, R. S. Katiyar, A. Cantarero, A. Soukiassian, V. Vaithyanathan, J. H. Haeni, W. Tian, D. G. Schlom, K. J. Choi, D. M. Kim, C. B. Eom, H. P. Sun, X. Q. Pan, Y. L. Li, L. Q. Chen, Q. X. Jia, S. M. Nakhmanson, K. M. Rabe and X. X. Xi, *Science* **2006**, *313*, 1614.

[2] C. Beekman, A. A. Reijnders, Y. S. Oh, , S. W. Cheong, and K. S. Burch, *Phys. Rev. B* **2012**, *86*, 020403(R).

[3] H. Fukumura, H. Harima, K. Kisoda, M. Tamada, Y. Noguchi, and M. Miyayama, *J. Magn. Magn. Mater.* **2007,** *310*, E367.

[4] H. Fukumura, S. Matsui, H. Harima, T. Takahashi, T. Itoh, K. Kisoda, M. Tamada, Y. Noguchi, and M. Miyayama, *J. Phys.-Condens. Mat.* **2007**, *19*, 365224.

[5] R. Haumont, J. Kreisel, and P. Bouvier, *Phase Transit.* **2006**, *79*, 1043.

[6] R. Palai, H. Schmid, J.F. Scott, and R.S. Katiyar, *Phys. Rev. B* **2010**, *81*, 064110.

[7] M.K. Singh, H.M. Jang, S. Ryu, and M.H. Jo, *Appl. Phys. Lett.* **2006**, *88*, 042907.

[8] S. Kamba, D. Nuzhnyy, M. Savinov, J. Šebek, J. Petzelt, J. Prokleška, R. Haumont, and J. Kreisel, *Phys. Rev. B **2007**, 75*, 024403.

[9] R.P.S.M. Lobo, R.L. Moreira, D. Lebeugle, and D. Colson, *Phys. Rev. B* **2007**, *76*, 172105.

[10] P. Hermet, M. Goffinet, J. Kreisel, and P. Ghosez, *Phys. Rev. B* **2007**, *75*, 220102(R).

[11] H.M. Tutuncu, and G.P. Srivastava, *Phys. Rev. B* **2008**, *78*, 235209.

[12] M.N. Iliev, M.V. Abrashev, D. Mazumdar, V. Shelke, and A. Gupta, *Phys. Rev. B* **2010**, *82*, 014107.

[13] M.K. Singh, S. Ryu, and H.M. Jang, *Phys. Rev. B* **2005**, *72*, 132101.

[14] A.J. Hatt, N.A. Spaldin, and C. Ederer, *Phys. Rev. B* **2010**, *81*, 054109.

[15] R. Palai, R. S. Katiyar, H. Schmid, P. Tissot, S. J. Clark, J. Robertson, S. A. T. Redfern, G. Catalan, and J. F. Scott, *Phys. Rev. B* **2008**, *77*, 014110.